Extended Abstracts of the 2012 International Conference on Solid State Devices and Materials, Kyoto, 2012, pp634-635

B-7-2

Promising Bipolar and Unipolar Resistive Switching in Ti-Doped Yb_2O_3 Thin Film

Somnath Mondal[1], Fa-Hsyang Chen[1], Chih-Wei Wang[1], Jim-Long Her[2], Yasuhiro H. Matsuda[3], and Tung-Ming Pan[1*]

[1]Department of Electronic Engineering, Chang Gung University, Taoyuan 333, Taiwan, R. O. C.
[2] Division of Natural Science, Center for General Education, Chang Gung University, Taoyuan 333, Taiwan, R. O. C.
[3]Institute for Solid State Physics, The University of Tokyo, Chiba 277-8581, Japan
[*] Tel: +886-3-211-8800 Ext. 3349; Fax: +886-3-211-8507; e-mail:tmpan@mail.cgu.edu.tw

1. Introduction

Resistive random access memory (ReRAM) devices as a scalable nonvolatile memory that can compete with embedded dynamic random access memory (DRAM) and Flash memory are in tremendous need for next generation memory application [1]. Such devices are of particular interest due to lower operation power, nondestructive readout, and low fabrication cost with CMOS integration. Varity of materials and models for resistive switching (RS) characteristics have been suggested for last few years [2]. However, two dominant "interface" and "filament" type RS mechanisms have been modeled to clarify the driving mechanism [3]. Recently, the Yb_2O_3 film has shown promising RS effect for future ultrahigh density memory applications [4]. For the real implementation to use Yb_2O_3-based ReRAM, its switching behavior needs to be fully controlled. In this study, the Ni/Ti-doped Yb_2O_3/TaN ReRAM device has been studied. This device exhibited both bipolar and unipolar RS behavior. In reliability test, the device showed good endurance and data retention characteristics. In addition, a plausible mechanism is proposed for different RS behaviors in Ti-doped Yb_2O_3 based ReRAM devices.

2. Experiment

A 30-nm Yb_2O_3 thin films with different Ti doping concentrations were deposited on TaN/SiO_2/Si substrates at room temperature by rf magnetron sputtering using both Yb and Ti targets. The atomic concentration of the Ti in one sample was 5%, while the other sample was highly doped (>5%). A 100-nm Ni top electrode was deposited on the oxide films by thermal evaporation technique. Fig. 1 shows the schematic of the device and the HRTEM confirms the thickness of the oxide film. The electrical measurements were performed by Agilent E5260A semiconductor parameter analyzer.

3. Results and discussion

Fig. 2 shows the XRD patterns of the Yb_2O_3 film for different Ti concentrations. No reflection peak from Yb_2O_3 confirms the amorphous phase of the film and corroborates well with TEM result. The transition between high and low resistance state of Ti-doped Yb_2O_3 devices was observed by different dc voltage sweeping operation. The stable bipolar (Fig. 3) and unipolar (Fig. 4) RS were found in the device for below and above 5% of Ti concentration, respectively. The driving mechanisms of different RS modes in the Ti-doped Yb_2O_3 devices are investigated. The high resistance state (HRS) current conduction in both devices is dominated by Schottky emission mechanism (Fig. 5 and 6). The barrier heights at the TaN/oxide interface are extracted by extrapolating the electric field to zero from Fig. 7 to be 0.83 and 1.58 eV for 5% and >5% of Ti-doped Yb_2O_3 devices, respectively. At low resistance state (LRS), the current conduction exhibits Ohmic behavior, which is consistent with the conducting filament model [3]. We consider that bipolar RS behavior is due to percolation of oxygen vacancies and other ionic/electronic defects within or near the interface area in 5% Ti device, while the oxygen migration between two metal electrodes in heavily doped devices exhibits the unipolar switching. The temperature dependent resistance value of both HRS and LRS are shown in Fig. 8. The weak semiconducting behavior of unipolar devices in LRS confirms the filamentary conduction by oxygen ions [4]. The reset behavior in unipolar switching mode is believed to be related to the rupture of the conducting filament by local Joule heating, while the same is due to the annihilation of oxygen defects. The schematic of the different reset mechanisms in RS are shown in Fig. 9. The set/reset voltage uniformity of the bipolar and unipolar mode memory devices are shown in Fig. 10 and 11, respectively. The reliability of switching endurance and data retention was tested. Fig. 12 and 13 show the switching endurance characteristics for DC and pulse switching operation, respectively. The data retention characteristics of the devices are shown in Fig. 14. These results reveal that the Ti-doped Yb_2O_3 is promising for next generation memory applications.

4. Conclusions

In summary, the resistive memory switching characteristics in Ni/Ti-Yb_2O_3/TaN ReRAM cell has been investigated. The resistive switching mechanism changes from bipolar to unipolar mode with increase in Ti-doping concentration. A plausible driving mechanism is proposed to explain this behavior. Furthermore, the reliability of the memory cell is studied for practical applications.

References

[1] L. Zhang, R. Huang, D. Gao, P. Yue, P. Tang, F. Tan, Y. Cai, and Y. Wang, IEEE Trans. Electron Devices **58** (2011) 2800.
[2] U. Russo, D. Ielmini, C. Cagli, and A. L. Lacaita, IEEE Trans. Electron Devices **56** (2009) 186.
[3] M.-C. Chen, T.-C. Chang, C.-T. Tsai, S.-Y. Huang, S.-C. Chen, C.-W. Hu, S. M. Sze, and M.-J. Tsai, Appl. Phys. Lett. **96** (2010) 262110.
[4] H.-C. Tseng, T.-C. Chang, J.-J. Huang, P.-C. Yang, Y.-T. Chen, F.-Y. Jian, S. M. Sze, and M.-J. Tsai, Appl. Phys. Lett. **99** (2011) 132104.

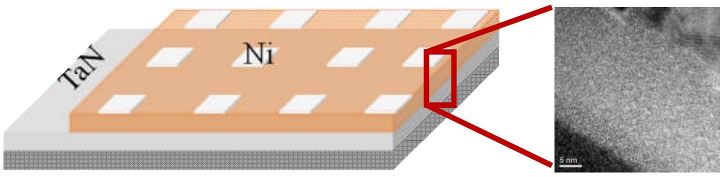

Fig. 1. Schematic of Ti-doped Yb_2O_3 memory cell. The zoom area shows the HRTEM image of the device.

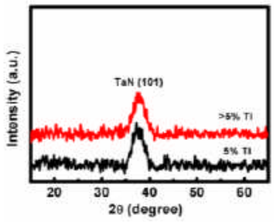

Fig. 2. XRD patterns of Ti-doped Yb_2O_3 thin film.

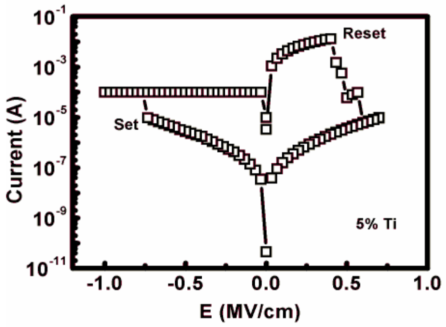

Fig. 3. Bipolar resistive switching in 5% Ti-doped Yb_2O_3 memory cell.

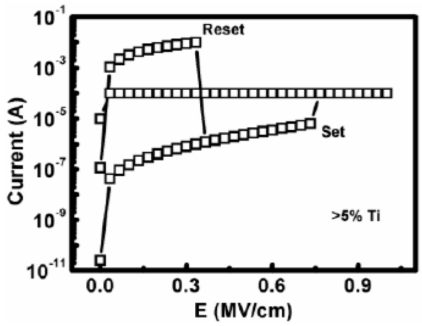

Fig. 4. Unipolar resistive switching in highly doped Yb_2O_3 memory cell.

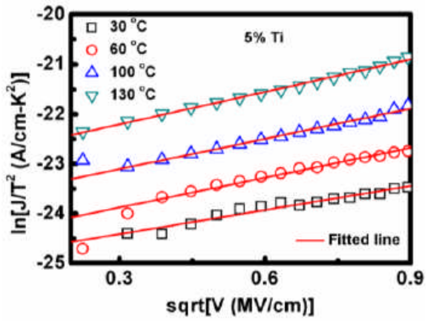

Fig. 5. HRS Schottky conduction mechanism in bipolar memory cell.

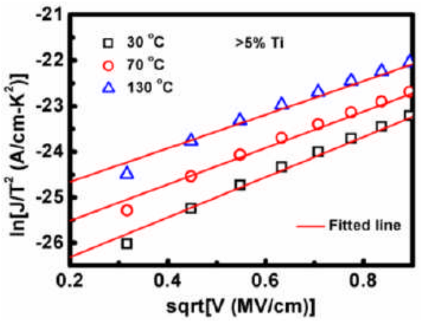

Fig. 6. HRS Schottky conduction mechanism in unipolar memory cell.

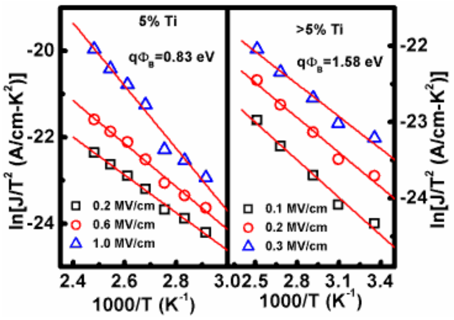

Fig. 7. Arrhenius plot of Schottky conduction in unipolar and bipolar memory cells.

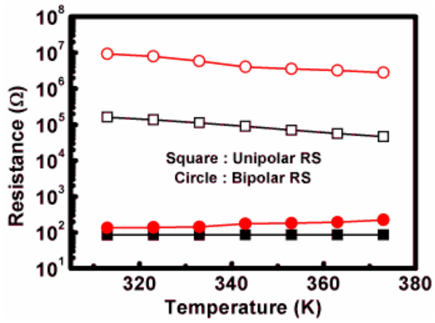

Fig. 8. HRS and LRS resistances as a function of temperature for unipolar and bipolar memory cells.

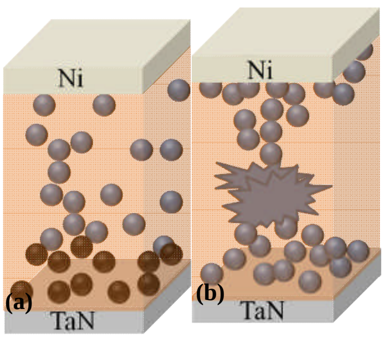

Fig. 9. Schematic of the reset process in (a) bipolar and (b) unipolar mechanisms.

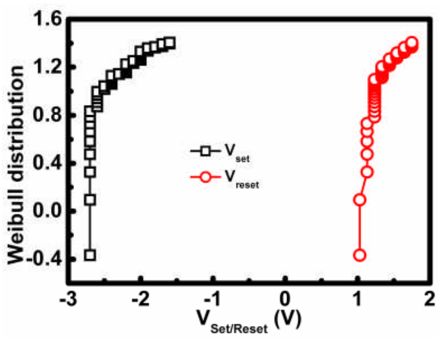

Fig. 10. Weibull distribution of set/reset voltage in unipolar switching device.

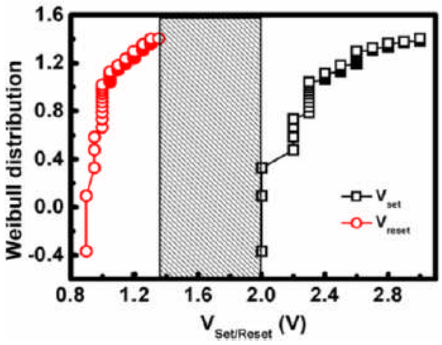

Fig. 11. Weibull distribution of set/reset voltage in bipolar switching device.

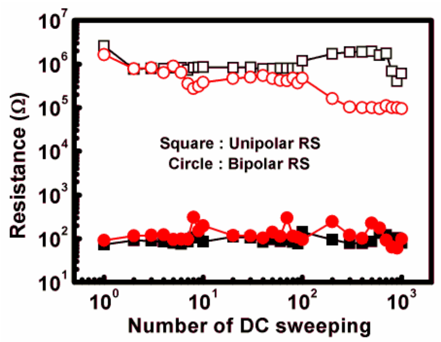

Fig. 12. DC switching endurance of Ti-doped Yb_2O_3 memory cell.

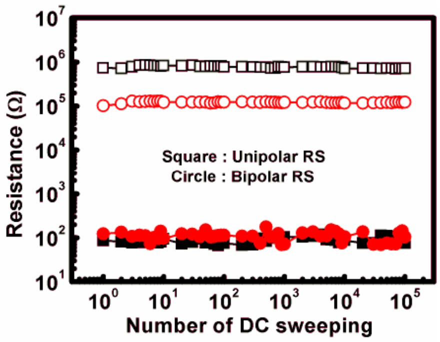

Fig. 13. Pulse switching endurance of Ti-doped Yb_2O_3 memory cell.

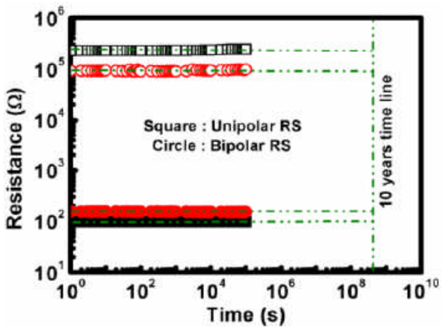

Fig. 14. Retention characteristics of Ti-doped Yb_2O_3 memory cell at room temperature.